Deformation in the heat affected zone during spot welding of a nickel-based single crystal

O. M. Barabash,[a] S. S. Babu, S. A. David, J. M. Vitek, and R. I. Barabash
Metals and Ceramics Division, Oak Ridge National Laboratory, Oak Ridge, Tennessee 37831

(Received 2 January 2003; accepted 15 April 2003)

Constrained melting and solidification and associated thermal cycling during welding produces extensive microstructural changes. Such changes are observed during spot welding of single-crystal Ni-based superalloy TSM-75. Analysis of Laue diffraction patterns attained from the heat-affected-zone indicates the presence of a high density of dislocations. Dislocation rearrangement results in local rotations around the [100] direction, which is perpendicular to the temperature gradient. These dislocations exist over a large fraction of the heat-affected zone. The analyses also showed that the dislocation density was maximal near the fusion line and gradually decreases with an increase in the distance from the fusion line. The dislocation density increased with the cooling rate. © *2003 American Institute of Physics.* [DOI: 10.1063/1.1579863]

INTRODUCTION

The heat-affected zone (HAZ) near the fusion zone (FZ) is the unmelted zone that is thermally affected by the thermal cycling during local melting and solidification.[1,2] The exact definition of the true HAZ is often confusing. In alloys that exhibit solid state transformation, the region that experiences such transformation due to the weld thermal cycle can be often identified by metallographic techniques. Sometimes hardness profiles can also be used to identify, on a microscopic scale, the extent of the HAZ. In single phase material, if the alloy shows grain growth effects, the extent to which grain growth occurs, and hence the extent of the HAZ, can be identified by metallographic techniques. During welding in all of these cases, the unmelted HAZ also experiences thermal stresses. The thermal stresses can be locked in as residual stress or they may relax by plastic deformation. In alloys that show solid state transformation, this secondary effect of strains due to the relaxation of thermal stresses may extend beyond the microstructural changes due to the solid-state transformation in the HAZ. Since the HAZ properties control the performance of the overall weld, there is a need to describe the HAZ from both microstructural and plastic deformation characteristics. In this article, the plastic deformation characteristics in the HAZ of a spot-welded, single-crystal nickel-based superalloy were characterized with Laue diffraction analysis.

Most Ni-based superalloys consist of γ solid solution (Ni based) with dispersed precipitates of γ' phase. The volume of these particles may reach 65%–75%. It is very important that at high temperatures above the γ' solvus temperature near the fusion zone, these γ' precipitates dissolve completely, leading to a single phase γ region. As a result, this single γ-phase region may exhibit lower strength. This soft region may experience plastic deformation on cooling due to the generation of thermal stresses that are higher than the yield strength. This deformation may lead to relaxation of thermal stresses. However, it is important to note that the above relaxation will also be influenced by the precipitation of γ' phase during cooling. Detailed analysis of the dislocation structure in the HAZ will enable one to define the extent of a true HAZ, and improve our understanding of physical processes taking place during welding and weld cooling of Ni-based alloys.

EXPERIMENTAL PROCEDURE

Analysis of the HAZ during spot welding of single crystal, nickel-based TSM-75 superalloy was performed. The composition of the alloy is (wt. %): Co-12.0, Cr-3.0, Mo-2.0, W-6.0, Ta-6.0, Al-6.0, Re-5.0, Hf-0.1 and balance nickel. The γ' solvus temperature for this alloy is (Ref. 3) ~1300 °C. A vertical section of the multicomponent phase diagram for this alloy, calculated using ThermoCalc[4] and the Ni-DATA[5] database, agrees with this temperature (Fig. 1). According to this calculation the solvus, solidus, and liquidus temperatures are 1323°, 1356°, and 1410 °C, respectively. The temperature interval between the solvus and solidus is 33°. As a result, the width of the single-phase γ region in the HAZ may not be large and will depend on the thermal gradient. During cooling below the solvus temperature, the alloy becomes two-phased (γ/γ') with 60–65 vol % γ' phase.

The welding experiments were carried out on the end of a single crystal rod that was 60 mm long and 13 mm in diameter. The single crystal sample microstructure had a dendrite structure [Fig. 2(a)]. Dendrites were oriented along the [010] sample axis (±2.5°). Spot welds were made on the rod using the gas tungsten arc process (on the plane perpendicular to the [010] axis). Two samples were prepared with different cooling conditions. In one case the arc was on for 17 s and then was switched off immediately so that the sample was rapidly cooled (sample B) and in the other case the arc was turned off gradually by ramping down the current

[a]Author to whom correspondence should be addressed; electronic mail: barabashom@ornl.gov

 © 2003 American Institute of Physics

Downloaded 04 Sep 2009 to 160.91.157.167. Redistribution subject to AIP license or copyright; see http://jap.aip.org/jap/copyright.jsp

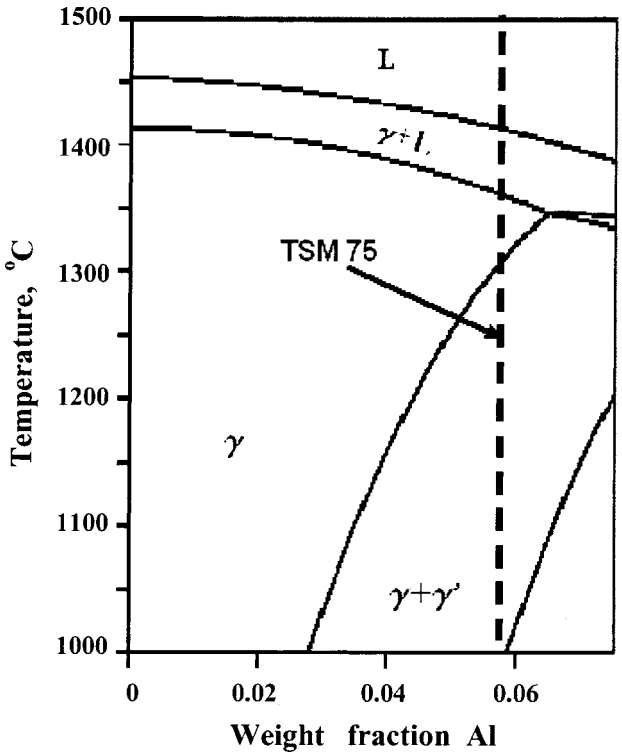

FIG. 1. Calculated section of the multicomponent phase diagram at a fixed concentration of 3Cr, 12Co, 2Mo, 6W, 5Re, 6Ta, 0.1Hf, and varying Al (0–12%) and Ni (65.9%–53.9%).

for 25 s (sample A). Since sample A was made with a gradually decreasing weld current, the cooling rates are expected to be lower than in sample B.

The HAZ was analyzed by cutting the samples on the (001) plane, through the cylinder axis and polishing electrolytically to remove surface damage. The structure of the HAZ was analyzed by optical microscopy and Laue diffraction. Laue images were obtained from different locations along the sample axis at different distances from the fusion line. The beam diameter for the Laue diffraction experiments was approximately 0.4 mm. As will be shown, this is considerably larger than the size of the HAZ when determined optically, but smaller than the HAZ when defined by the extent of deformation. Coordinates of the spots are listed in Table I and are shown schematically in Fig. 3. To get the exact positions of the spots, a Laue image from the edge of the sample was taken and this position was then used as a reference.

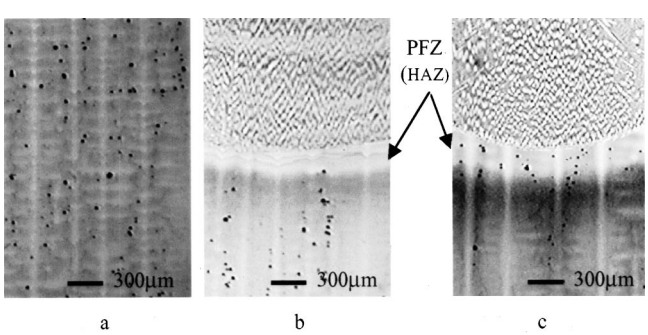

FIG. 2. Microstructure of TSM75 single crystal samples: (a) dendrite microstructure of base material; (b) fusion zone and PFZ(HAZ) in sample A; (c) fusion zone and PFZ(HAZ) in sample B.

TABLE I. Size of heat affected zone (R) from x-ray data.

Sample A		Sample B	
Spot No.	Distance from fusion line (mm)	Spot No.	Distance from fusion line (mm)
1	1.75	1	3.22
2	1.25	2	1.95
3	0.75	3	1.95
4	0.25	4	1.35
5	0.1	5	1.35
6	0.1	6	0.85
7	−0.1	7	0
8	−0.3	8	−0.3
R	1.5	R	2.65

In Laue diffraction, the incident and scattered beams each define a line in reciprocal space. The length of the line is determined by the wavelength of the radiation. Since white beam conditions are used, a continuous range of incident and scattered reciprocal space vector lengths are present. Furthermore, higher orders of reciprocal lattice points [for example $(00h)$, $(002h)$, $(003h)$, $(004h)$ etc.] lie along the same direction and therefore will lead to scattering at the same pixel on the detector (Fig. 4). To analyze the white beam intensity distribution from a deformed grain, *unit* vectors in each direction of scattering, $\hat{\mathbf{k}}=\mathbf{k}/|\mathbf{k}|$, are introduced. Also, a special misorientation vector $\mathbf{m}$ near a Bragg reflection ($\mathbf{m}=\hat{\mathbf{k}}-\hat{\mathbf{k}}_{hkl}$) is defined.[6,7] The misorientation vector $\mathbf{m}$ gives the difference between the unit vector parallel to the Bragg reflection (hkl) and an arbitrary direction in its vicinity (Fig. 4).

RESULTS

The final microstructure of samples A and B are shown in Figs. 2(b) and 2(c). The microstructures showed some interesting features. The width of the HAZ when defined by optical contrast was equal to 280 μm in sample B and was

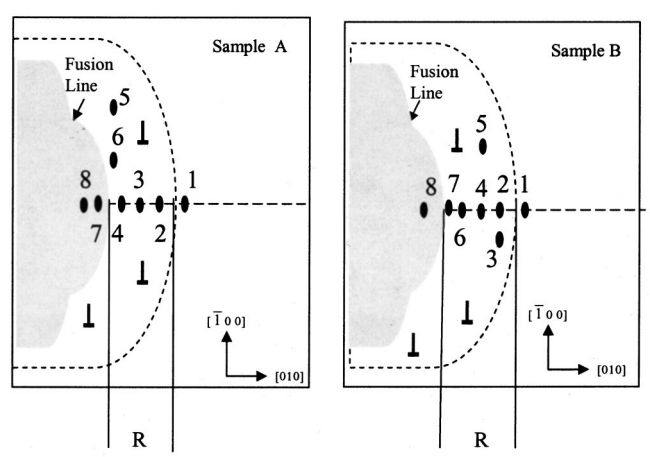

FIG. 3. Spot positions at which Laue patterns were taken from samples A and B. Scales for the two schematic diagrams are different.

Downloaded 04 Sep 2009 to 160.91.157.167. Redistribution subject to AIP license or copyright; see http://jap.aip.org/jap/copyright.jsp

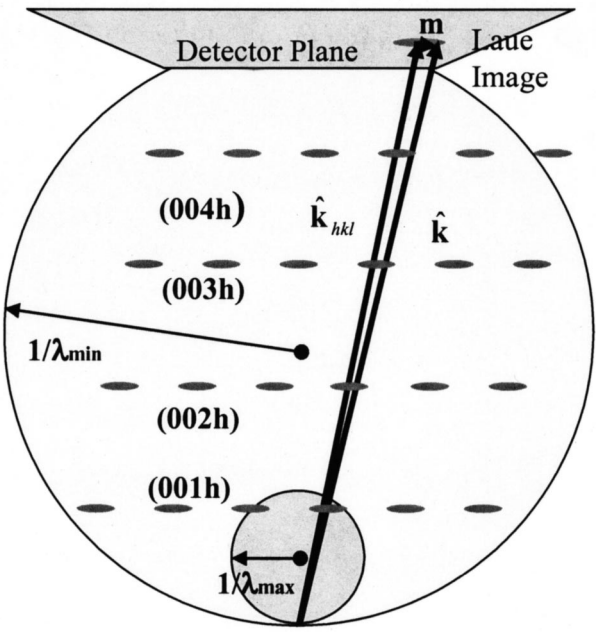

FIG. 4. Scheme of Laue diffraction illustrates that reciprocal lattice points (00h), (002h), (003h), (004h), etc. are scattered towards the same pixel on a detector. Laue image characterizes the misorientation distribution within the irradiated volume.

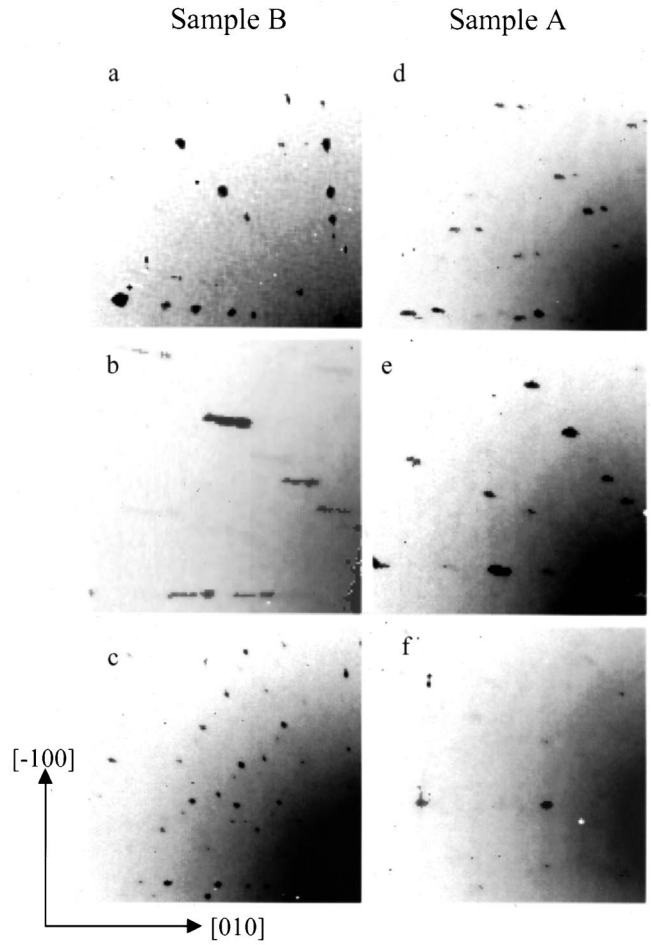

FIG. 5. Experimental Laue patterns from sample B at (a) position 1; (b) position 7; (c) position 8; and from sample A at (d) position 2; (e) position 4; (f) position 7.

larger than that in sample A (200 μm). This result is in apparent contradiction to traditional behavior, but can be explained as follows. Since sample A cooled more slowly, the extent of reprecipitation of γ' in the HAZ during cooling will be greater than in sample B. This will render a smaller precipitation-free zone (PFZ) (as observed by optical microscopy) near the fusion line and will result in an apparently smaller HAZ. Microscopy also confirmed the results of Laue diffraction in that the HAZ retains its single crystal nature. In the HAZ closer to the fusion line, there were indications of homogenization of the base material cast structure. In the FZ there was a clear indication of solidification proceeding epitaxially from the fusion line and having the same orientation as the base material. This was confirmed by Laue analysis. Microstructural analysis indicated that the fusion zone far from fusion line consists of several grains.

Laue images show that after melting the sample retained its single crystal nature near the fusion line. No grains due to recrystallization was observed. At large distances from the fusion line (more than 1.75 mm for sample A and 3.35 mm for sample B), in the HAZ, the Laue pattern consists of sharp spots. This indicates that at this distance there is no plastic or elastic strain [Fig. 5(a)]. As the analyzed locations were moved closer to the fusion line, the Laue images changed dramatically. For both samples the Laue spots changed from sharp points to elongated streaks [Figs. 5(b), 5(d), and 5(e)]. For sample B, which was cooled much faster, the changes in the Laue pattern were more pronounced than in sample A. The maximum length of the Laue spots was observed near the fusion line [Figs. 5(b) and 5(e)]. The shape of Laue images remained elongated at some distance into the fusion zone. It should be pointed out that the Laue images located along the [010] direction have streaks in the same direction [010] [Figs. 5(b) and 5(e)]. Furthermore, as one moves into the fusion zone, the Laue images obtained were sharp once again, similar to the nondistorted single crystal base material [Figs. 5(c) and 5(f)]. If the HAZ width is defined by the extent of plastic/elastic strain, as measured by Laue diffraction, then the rapidly cooled sample (B) has a larger HAZ. This is reasonable since the stresses that develop in the rapidly cooled sample are larger and have little time for relaxation.

DISCUSSION

It has been shown[6–8] that the shape of the Laue image is related to the plastic and elastic state of the sample. During welding, the temperature gradients in the sample generate strains. These strains result in the formation of dislocations, which lead to a relaxation of the thermal stresses. Rearrangement and movement of the dislocations also result in the formation of subboundaries and a corresponding rotation of the lattice planes. It is known that nonlinear thermal gradients, compared to linear gradients, result in the formation of higher dislocation densities.[9] In the first approximation, the density of dislocations (n) that leads to stress relaxation is

Downloaded 04 Sep 2009 to 160.91.157.167. Redistribution subject to AIP license or copyright; see http://jap.aip.org/jap/copyright.jsp

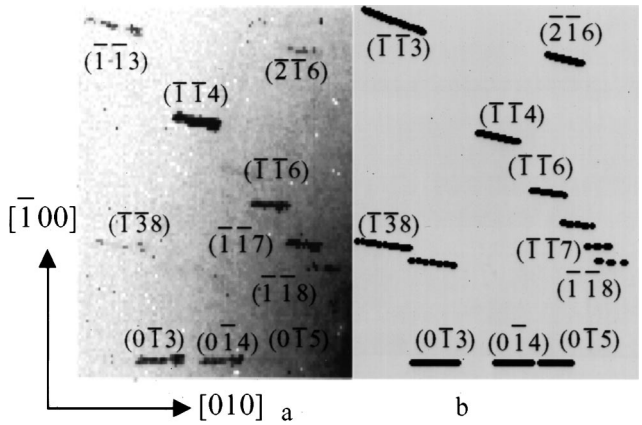

FIG. 6. Experimental (a) and simulated (b) Laue pattern corresponding to the plastic deformation with rotation axes around the [100] direction.

roughly proportional to the variation of the temperature gradient $\delta\nabla T$, lattice parameter a, and thermal expansion coefficient α:[9]

$$n \propto \alpha \delta \nabla T / a.$$

The local sample rotation due to dislocation formation and movement leads to distortion of the Laue diffraction spots and the extent of distortion can be measured quantitatively by the Laue method. By comparing measured patterns with simulated ones, one can quantitatively determine the elastic and plastic strain in different regions of the single crystal.[6,7] In this study Laue images have been simulated for different possible dislocation arrangements and compared with the experimental results. Thus we could identify the arrangement of dislocations in the HAZ of the single crystal weld specimen. The best fit to the experimental observations is shown in Fig. 6(b).

Also, as dislocations are rearranged to relax the thermal stresses, they form subboundaries that in turn reduce the energy of the crystal. According to the classic Mughrabi model,[10–12] cells with different orientations form and they are separated by subboundaries, which are formed by tilt dislocation walls. Each boundary results in a rotation between two neighboring mosaic blocks.[13,14] This rotation leads to the splitting of Laue images into a streak containing several small spots. This is shown in Fig. 7(a) as a contour map of the reflection $(0\bar{1}4)$. Hence the nature of the dislocations and subboundaries can be understood from the characteristics of the streaking of the Laue images.

The simulated dislocation arrangement that led to the best fit to the experimental pattern consisted of dislocations distributed equally over the octahedral slip systems with the following Burgers vectors and slip planes normals: $b=[0\bar{1}\bar{1}]$ and $N=(1\bar{1}\bar{1})$ or $N=(\bar{1}\bar{1}1)$; $b=[0\bar{1}1]$ and $N=(111)$ or $N=(\bar{1}\bar{1}1)$; $b=[1\bar{1}0]$ and $N=(\bar{1}\bar{1}1)$ or $N=(111)$; $b=[\bar{1}10]$ and $N=(\bar{1}11)$ or $N=(1\bar{1}\bar{1})$. All these slip systems are symmetrical with respect to the direction of the temperature gradient and have the same Schmidt factor of 0.408. Similar to the quantitative Mughrabi model[10] they result in a macroscopically uniaxial plastic deformation along the direction of the temperature gradient and create

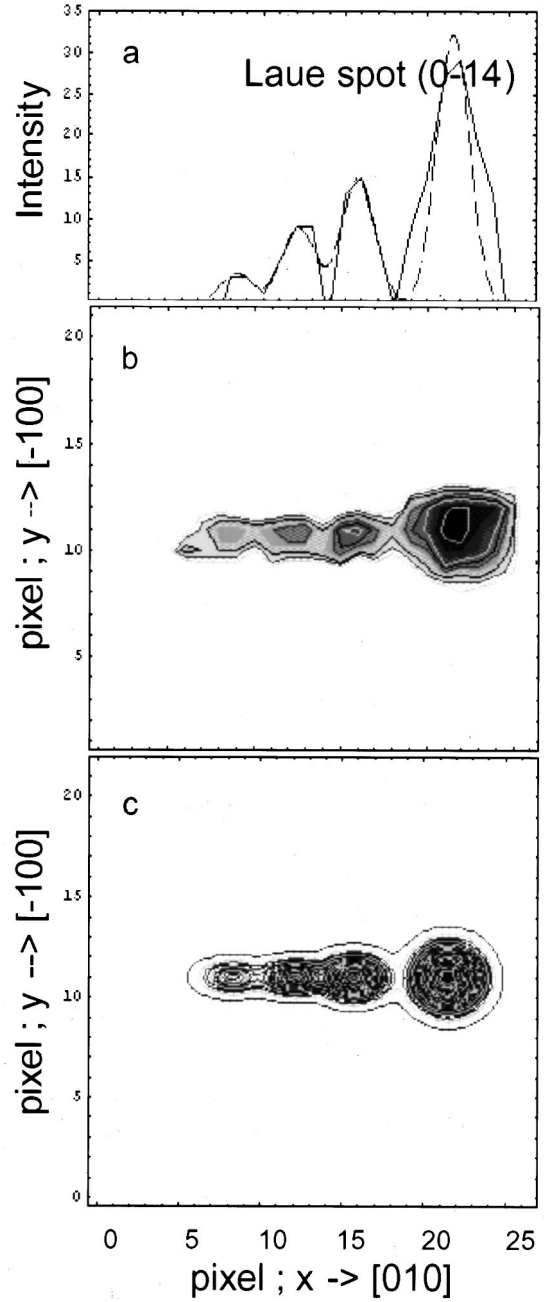

FIG. 7. Experimental and simulated $(0\bar{1}4)$ Laue images and intensity profiles for sample B, position 7: (a) experimental (solid line) and simulated (dashed line) intensity profiles along the split $(0\bar{1}4)$ Laue image showing intensity spikes; (b) experimental contour map of $(0\bar{1}4)$ Laue image consists of several spots; (c) simulated $(0\bar{1}4)$ Laue image corresponding to lattice rotation around [100] direction; (c) simulated $(0\bar{1}4)$ Laue image corresponding to lattice rotation around [100] direction.

local lattice rotations around the axis [100], perpendicular to the [010] sample axis. Maximal spread in misorientation in the HAZ reaches 1.7° and misorientation between neighboring scattering domains within the irradiated area is about 0.6°. The other four octahedral dislocation systems have a zero Schmidt factor with respect to the direction of the temperature gradient. Figure 8 shows the experimental variation in dislocation density from the fusion line into the HAZ for both samples A and B. The dislocation density decreases at

Downloaded 04 Sep 2009 to 160.91.157.167. Redistribution subject to AIP license or copyright; see http://jap.aip.org/jap/copyright.jsp

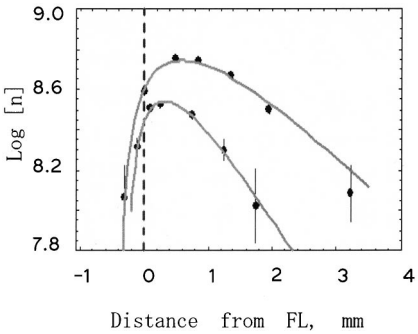

FIG. 8. Dependence of dislocation density on the distance from the fusion line (FL) along the axes of samples A and B. The dashed line indicates the position of the fusion line as determined optically.

large distances away from the fusion line and ultimately reaches the value for a dislocation density of the perfect single crystal base material. The dislocation density in the fusion zone decreases even more sharply with distance from the fusion line. These results enable the determination of the size of the heat affected zone (Table I and Fig. 3) in terms of the distance over which strains and deformation take place. This result also confirmed that for the sample B, with the higher cooling rate, the HAZ (as defined by the size of the plastically deformed zone) is larger than for sample A which was cooled slowly. This is a very critical point.

The higher level of stress results in a higher dislocation density. This explains the higher distribution of dislocation density along the sample axis in sample B than in sample A (Fig. 8). Optical microscopy shows the HAZ as the region where γ' dissolves in the matrix. The size of this region is quite small and is slightly larger in the rapidly cooled sample B ($\sim$280 μm) than in the slowly cooled sample A ($\sim$200 μm) [see Figs. 2(a) and 2(b)]. This is because the extent of reprecipitation of γ' upon cooling is greater in the slowly cooled sample. The optically identified HAZ is much less than the size of HAZ where deformation and stress relaxation take place. This difference in the size of the HAZ is due to the fact that dissolution of γ' is controlled by diffusion and takes place only at higher temperatures and at a lower rate (10–100 times) than the formation and motion of dislocations due to thermal stresses. Further investigation of the local dislocation distribution and local microstructure in the HAZ with higher spatial resolution synchrotron radiation is underway.

CONCLUSIONS

(i) It was established that the local melting and solidification of TSM75 Ni-based single crystal during welding results in the formation of a region in the HAZ with a high dislocation density near the fusion line. The size of the HAZ, as defined by either the extent of the precipitation free zone or the size of plastic/elastic strained region, and maximum dislocation density increase with increasing cooling rate.

(ii) The spatial variation of the dislocation density is not monotonic within this region. The dislocation density increases near the fusion line and has a maximum value near the fusion line. The dislocation density decreases as one proceeds away from the fusion line, into either the fusion zone or towards the base material.

(iii) Splitting of Laue spots demonstrates that dislocations group together, forming subboundaries and causing fragmentation and local rotation in the HAZ. Macroscopic rotation axes are parallel to the direction [100].

ACKNOWLEDGMENT

Research was sponsored by the Division of Materials Sciences and Engineering, Office of Basic Energy Sciences, U.S. Department of Energy, under Contract No. DE-AC05-00OR22725 with UT-Battelle, LLC.

[1] S. A. David and J. M. Vitek, Int. Mater. Rev. **34**, 213 (1989).
[2] S. A. David and T. Debroy, Science (Washington, DC, U.S.) **257**, 497 (1992).
[3] T. Kobayashi, Y. Koizumi, S. Nakazawa, T. Yamaguta, and H. Harada, in *Advances in Turbine Materials, Design and Manufacturing* (The Institute of Materials, London, 1997), pp. 766–773.
[4] B. Sundman, B. Jansson, and J.-O. Andersson, CALPHAD: Comput. Coupling Phase Diagrams Thermochem. **9**, 153 (1985).
[5] Ni-DATA, N. Saunders, ThermoTech Ltd., Surrey Technology Centre, 40 Occam Road, GuildfordGU2 5YH, UK, 2001, Vol. 5.
[6] R. I. Barabash, G. E. Ice, B. C. Larson, G. M. Pharr, K.-S. Chung, and W. Yang, Appl. Phys. Lett. **79**, 749 (2001).
[7] R. I. Barabash, G. E. Ice, and F. J. Walker, J. Appl. Phys. **93**, 1457 (2003).
[8] M. A. Krivoglaz, *Theory of X-Ray and Thermal Neutron Scattering by Real Crystals* (Plenum, New York, 1969), p. 402.
[9] A. Chernov, *Modern Crystallography* (Nauka, Moscow, 1980), Vol. 3, p. 410.
[10] H. Mughrabi, Acta Metall. **31**, 1367 (1983).
[11] T. Ungar, H. Mughrabi, D. Ronnpagel, and M. Wilkens, Acta Metall. **32**, 333 (1984).
[12] M. Wilkens, T. Ungar, and H. Mughrabi, Phys. Status Solidi A **104**, 157 (1987).
[13] F. R. N. Nabarro, *Theory of Crystal Dislocations* (Dover, New York, 1987).
[14] D. Hughes and N. Hansen, Acta Mater. **48**, 2985 (2000).

Downloaded 04 Sep 2009 to 160.91.157.167. Redistribution subject to AIP license or copyright; see http://jap.aip.org/jap/copyright.jsp